

Velocity predictions from a coupled one-dimensional/three-dimensional computational fluid dynamics simulation compared with measurements in the catalyst system of a firing engine

Benjamin, S.F. , Disdale, W. , Liu, Z. , Roberts, C.A. and Zhao, H.

Author post-print (accepted) deposited in CURVE June 2013

Original citation & hyperlink:

Benjamin, S.F. , Disdale, W. , Liu, Z. , Roberts, C.A. and Zhao, H. (2006) Velocity predictions from a coupled one-dimensional/three-dimensional computational fluid dynamics simulation compared with measurements in the catalyst system of a firing engine. International Journal of Engine Research, volume 7 (1): 29-40.

<http://dx.doi.org/10.1243/146808705X30486>

Copyright © and Moral Rights are retained by the author(s) and/ or other copyright owners. A copy can be downloaded for personal non-commercial research or study, without prior permission or charge. This item cannot be reproduced or quoted extensively from without first obtaining permission in writing from the copyright holder(s). The content must not be changed in any way or sold commercially in any format or medium without the formal permission of the copyright holders.

This document is the author's post-print version of the journal article, incorporating any revisions agreed during the peer-review process. Some differences between the published version and this version may remain and you are advised to consult the published version if you wish to cite from it.

CURVE is the Institutional Repository for Coventry University

<http://curve.coventry.ac.uk/open>

VELOCITY PREDICTIONS FROM A COUPLED 1D/3D CFD SIMULATION COMPARED WITH MEASUREMENTS IN THE CATALYST SYSTEM OF A FIRING ENGINE

S. F. Benjamin, W. Disdale, Z. Liu, C. A. Roberts and H. Zhao

School of Engineering, Coventry University, UK

Abstract

Velocity measurements were made in the catalyst system of a firing engine using a one component LDV system. The 1.4 litre engine was operated at 2000 rpm and 88% full load condition. Velocity pulsations were observed in one of the runners supplying the catalyst and downstream of the catalyst. The velocity pulsations measured downstream of the catalyst enabled the mean velocity profile to be found. Observations were compared with simulations obtained from a coupling of the Star-CD CFD code, which modelled the catalyst as a 3D component, with the Ricardo WAVE 1D engine-cycle simulation code. The velocities in the runners were predicted to fluctuate between –65 m/s and 240 m/s. The observed velocity showed a similar pulse shape but a smaller magnitude of reversed flow. The velocities downstream of the catalyst were predicted to fluctuate between –5 and 22 m/s. The observed velocities showed smaller amplitude pulsations and significantly lower magnitudes of reversed flow, consistent with the input runner observations. The coupled simulation was shown to give good qualitative agreement with measurements, with quantitative predictions being most accurate near to the catalyst centre but less accurate at locations closer to the outer wall.

Nomenclature

| | |
|-----------------|--|
| f_s | frequency shift between beams of LDA system (Hz) |
| F | fringe spacing (m) |
| L | monolith length (m) |
| Δp | pressure loss (Pa) |
| u | superficial velocity in channel axis direction (m/s) |
| $ V $ | superficial velocity magnitude (m/s) |
| α, β | permeability coefficients |
| θ | angle between beams of LDA system (°) |
| λ | wavelength of laser light (m) |
| V_D | magnitude of effective fringe drift velocity (m/s) |

1.0 Introduction

Automotive catalyst performance is highly dependent upon the flow distribution. When the catalyst is close-coupled to the engine, the flow distribution changes markedly during the two revolutions of the engine that comprise the engine cycle in a four-cylinder engine. The individual runners that duct the exhaust gases from the engine supply high velocity jets to parts of the catalyst in turn, dependent upon the design of the diffuser upstream of the catalyst. If this process can be successfully modelled, then design of the diffuser and catalyst system can be achieved without the need for prototyping. Often, the design is constrained by the requirements of the component manufacturing process and by space in the engine compartment. Alternative designs can be assessed and compared much more cheaply if a reliable model for performance prediction is available.

In the last ten years there have been a number of studies published attempting to model the flow in a close-coupled catalyst. An early study [1] of the CFD prediction of pulsating flow in a catalytic converter was carried out by Bressler et al. in 1996. Cho et al. reported a similar study [2] in 1998. In both of these studies the flow was provided by a pulse generator rather than an engine. Some recent work has shown [3, 4] that the behaviour of the engine under motoring conditions is significantly different from that under firing conditions. Many recent studies have concentrated on firing engines. There is work in the literature by Zhao et al., [5] that suggests that pulsations from an engine do not pass through a catalyst monolith mounted in an under floor configuration. Measurements made here previously by hot-wire anemometry [6] have, however, demonstrated that even modest pulsations from a cold flow test rig do pass through monolith substrates and clearly in the case of a close-coupled catalyst on a firing engine, where velocity pulsations are of much higher amplitude, the pulsations will be transmitted by the catalyst. The work reported in [5] was extended by Bai et al., [7] to close-coupled catalysts, and pulses were measured at the catalyst exit under firing conditions. These authors discussed the non-uniformity of the velocity distribution in their paper and attempted to identify the most suitable location for the oxygen sensor in their particular exhaust geometry. Park et al. [8] reported some similar measurements on a dual brick system and additionally presented CFD predictions for their particular geometry. They concluded that the primary flow of the blow down process governs the overall flow characteristics of the exhaust.

A coupled model has been developed that can make predictions of velocity in the catalyst system for both motored and firing engine conditions [9]. The coupled model links the engine cycle simulation code Ricardo WAVE with the CFD code Star-CD. The coupled model should provide advantages over conventional CFD because the input to the runners in the CFD model, which controls the exhaust flow, is simulated. This avoids the need to arbitrarily specify the inputs to the runners at the model inlet boundary.

In the paper [9] where the coupled model was described, predictions were compared with velocity data measured in the catalyst system downstream of a motored engine. Both temporal pulse shapes and spatial velocity profiles were measured and compared. Agreement was found to be quite good. One single point measurement in a firing engine was presented in that paper. It thus remains necessary to more fully validate the coupled simulation model against data obtained under firing engine conditions. This work is reported here, with particular emphasis on the gathering of the experimental data. A simple laser Doppler velocimetry (LDV) system was used to make measurements of the velocity pulsations in a runner leading from the engine port to the catalyst diffuser, and also downstream of the catalyst monolith. The mean velocity profile was also obtained downstream of the catalyst brick across the catalyst outlet face. The LDV technique [10] is the technique of choice for velocity measurements in firing engine work as it is not intrusive and the problems associated with velocity measurements at high temperatures are minimised. The LDV technique is also useful where significant reverse flows are encountered.

This paper reports measurements that were carried out specifically to provide data for model validation. The work described here extends the validation of the coupled model to firing engine conditions, with measurements being made for a typical engine operating condition.

2.0 Test rig and experimental technique

The geometry of the experimental set up is fully described elsewhere [4]. Figure 1 shows schematically a plan view that indicates the location of the engine, runners and measurement axes relative to the catalyst monolith. Figure 2 shows a photograph of the experimental test rig. Four runners supplied the flow to the catalyst system. Each had an approximately oval cross section with 36 mm major axis and 24 mm minor axis. A block containing flow straighteners and optical windows was

present in the engine test rig between the engine outlet ports and the manifold. The runners from the manifold entered a small diffuser upstream of the catalyst. The catalyst monolith was 120 mm in diameter and 120 mm in length. A chamber was fitted downstream of the catalyst monolith, between the brick and the exhaust duct, that was 126 mm diameter and was fitted with viewing windows 6 mm thick of polished fused quartz. The measuring plane through the windows was approximately 30 mm from the catalyst brick exit, i.e. far enough to avoid jets from the individual channels [11].

The engine used for the experiments was a 1.4 litre 4-cylinder 16 valve gasoline-fired automotive engine. The condition for the velocity measurements was 2000 rpm, 88% of full load, with 70 Nm torque approx. The engine was mounted on a test bed and linked to a Froude-Consine eddy current dynamometer controlled with a Texcel V4 control system.

The flow velocities were measured with an LDV system probe of the fibre optic type. It had 120 mm focal length and 16 mm beam spacing. Allowing for the geometry of the test rig, this could measure up to a maximum of 93 mm away from the inside of the viewing window. It was thus not possible to measure fully across the diameter but it was possible to probe well beyond the central axis. The half angle of the 514 nm argon-ion laser beam intersection was 3.81° . The LDV measuring volume was estimated to have length of about 2.2 mm. A water-cooled jacket support allowed the probe to be rigidly attached to the catalyst system without overheating the LDV probe. This was necessary because significant engine vibration was transmitted to the exhaust and catalyst system.

For an LDV system, the basic equation is,

$$F \sin (\theta / 2) = \lambda / 2$$

For this system, the half angle ($\theta / 2$) between the beams is 3.81° and wavelength λ is 514 nm so that fringe spacing F is 3.868 μm . Furthermore,

$$V_D = F f_s$$

For this system, the frequency shift f_s between the two beams is 10 MHz so that the effective fringe drift velocity V_D is 38.68 m/s. The velocities downstream of the catalyst (predicted to pulse between -5 and 22 m/s) can be readily measured with the normal signal filter settings for this system of 5 to 30 MHz. The velocities upstream of the catalyst in the runners, however, are predicted to pulse between

–65 and 240 m/s. This required an upper filter limit of 90 Hz for measurements of the main peak and additional measurements with other filter settings and the probe reversed relative to the flow direction to measure the high reverse flows. Table 1 indicates the velocity measuring capabilities of this system, which are dependent upon signal filter settings.

The signal processing system was a TSI IFA 750; the rotating machinery resolver was also supplied by TSI. This system, together with a shaft rotary encoder, enabled the 720° of crank angle per two engine revolutions to be divided into 124 spans, each of 5.8°, into which the velocity data were assigned. At 2000 rpm, 5.8° change in crank angle corresponds to a time interval of 0.48 ms. Temporal pulse shapes were measurable from ensemble averages of velocity measurements collected over multiple cycles. In excess of 3k data points were obtained at each measurement location within a few seconds. The maximum amount of data recorded at any one location in one test was 16k data points.

The seeding of the fuel was achieved using the method described by Zhao et al. [12], who suggested titanium isopropoxide, 5 – 8 %, mixed into the fuel to generate titanium dioxide particles on combustion. In this work it was found that the lower end of this range, 5 – 6 % by volume, was most satisfactory. The measured amount of titanium isopropoxide was simply poured into the fresh fuel prior to an experiment. The engine was run until the water outlet temperature reached 80° C. The engine was then turned off and the viewing window was replaced with a fresh quartz glass. The engine was restarted and measurements were made and continued until failure to obtain data, usually due to fouling of the window. The window was then replaced again, the engine was restarted and experiments were continued unless the engine showed signs of running roughly, which was sometimes noticed after extended periods of experimentation. In that case, the tests were suspended and the engine was allowed to cool thoroughly before tests proceeded. The spark plugs, which became coated on one side with titanium dioxide deposits after extended tests, were cleaned periodically. The engine was purged for several minutes with undoped clean fuel after each batch of tests. It was also necessary periodically to clean the engine fuel injectors. There was no visual evidence of blocking of the catalyst itself, even after long periods of testing.

3.0 Coupled model and model predictions

3.1 Coupled model

The coupled model was first described by Liu et al. [9]. Figure 3 shows a schematic diagram of the 1D WAVE model and Figure 4 shows the mesh for the 3D CFD model. These are the two components of the coupled simulation. WAVE is linked to the Star-CD CFD model at five boundaries. These are the four runner inlets and the exit from the outlet pipe. WAVE was the controlling programme in the coupled simulation, where the procedure was as follows:

- (a) WAVE calculates its own time step size, sub-stepping if required within the fixed Star-CD time step size.
- (b) WAVE solves explicitly the governing equations in its piping system up to the end of a Star-CD time step.
- (c) WAVE provides the boundary conditions, time-averaged over the Star-CD time step. These boundary conditions are the flux at the WAVE/Star-CD interface and the state boundary conditions, i.e. density and temperature of the discretisation volume adjacent to the interface. They are provided to Star-CD via user subroutines.
- (d) Using both the flux and state boundary conditions that have been provided by WAVE for the end of the Star-CD time step, Star-CD then solves the 3D flow field.
- (e) Star CD spatially averages the revised boundary conditions and passes them back to WAVE via RSimlink coding.
- (f) Steps (b) to (e) are repeated for each time step through the co-simulation until the specified completion time is reached.

The connecting interface between the two models at each of the five boundaries referred to above (indicated in Figures 3 and 4) was assumed to be a flat plane normal to approximately 1D flow. In the WAVE model shown in Figure 3 the 1D network linking the five junctions is termed a ‘shadow network’ and it was this that was replaced by the 3D CFD model in the second phase of the co-simulation. The purpose of the shadow network was to reduce the cpu time required to obtain a converged coupled solution. In the coupled simulation, WAVE modelled two cases. Case 1 used the shadow network and was run for 20 engine cycles to obtain a converged solution. The flow field at the

end of this provided the initial field for Case 2. In Case 2, the 3D CFD model replaced the shadow network and the two codes performed the coupled simulation, as outlined above. Case 2 was run for only 3 engine cycles, of which only the third was analysed. The simulations took two to three weeks on an SGI Octane workstation with a single R12000 processor and 2GB of RAM.

The 3D CFD model shown in Figure 4 contained about 220,000 cells. The cell layer in the mesh adjacent to the interface between WAVE and Star CD was increased in the axial direction to avoid numerical instability in the coupled simulation. All the surfaces of the mesh, except for the five plane boundaries, were defined as ‘non-slip’ adiabatic walls. The effect of chemical reaction on monolith temperature was not included in the model. The PISO algorithm [13] was used for the transient analysis. The time step was equal to 0.5° crank angle at 2000 RPM (i.e. 4.17×10^{-5} s approx.). The second order differencing scheme MARS (monotone advection and reconstruction scheme) [14] was used for momentum variables. The MARS scheme operates in two steps: reconstruction, which uses a TVD (total variation diminishing) scheme, and advection. First order upwind differencing was the chosen scheme for turbulence variables and enthalpy. The compressible high Reynolds $k-\varepsilon$ model was used as the turbulence scheme [14] and the ‘log wall function’ was used to treat the flow in the wall boundary layer. The catalyst monolith was modelled as a porous medium with appropriate prescribed flow resistance of the form

$$\frac{\Delta p}{L} = (\alpha |V| + \beta) \mathbf{u}$$

The transverse permeability coefficients were assigned values of 10^{-8} whilst in the direction of the channel the pressure loss was described by the Hagen-Poiseuille equation and hence permeability β was temperature dependent.

3.2 Model predictions

Figure 5 shows the mean (cycle-averaged) velocity at the catalyst exit predicted from the coupled model. The profiles for axes 1, 2 and 3 are compared. The locations of the 3 axes are shown in Figure 1. The predicted mean velocity distribution can be seen in Figure 5 to be spatially non uniform, i.e., maldistributed, but approximately axially symmetric.

Figure 6, from A to P, shows the predicted velocity distribution at the catalyst exit at various times over the 720° corresponding to two engine rotations. The engine firing order was 1-3-4-2 and the engine ports and runners are numbered as in Figure 1. For reference, Table 2 gives complete timing data for the engine. The exhaust valve closes 23° after exhaust TDC, the inlet valve closes 62° after BDC, the exhaust valve opens 39° before BDC and the inlet valve opens 22° before exhaust TDC.

Figures 6A to 6D show the evolution of the pulse supplied from runner 4. This occurs at a time just after compression TDC of cylinder 2. There is swirl of flow from runner R4 evident from 6A to 6B. Figures 6E to 6H show the evolution of the pulse from runner 2. The peak occurs at a time just after compression TDC of cylinder 1. Figures 6I to 6L show the evolution of the pulse from runner 1. This occurs at a time just after compression TDC of cylinder 3. There is swirl of flow from runner R1 evident from 6I to 6J. Finally, Figures 6M to 6P show the evolution of the pulse from runner 3. This pulse occurs at a time just after compression TDC of cylinder 4. The angles stated on the figures are defined such that 360° corresponds to top dead centre of cylinder 1, as shown in Table 2. The predicted peak velocities from runners 1 and 4 spread over a crescent shaped area of the catalyst, due to the angle at which the jets from the runners impinge on the opposite diffuser wall and the catalyst inlet face. Runners 1 and 4 are the outside runners, see Figure 1, and perform similarly due to symmetry. The peak velocities from runners 2 and 3 are more highly localised, again due to the angle at which they enter the diffuser upstream of the catalyst. Runners 2 and 3 are the inside runners and again perform similarly due to symmetry.

Figure 7 shows the predicted cycle-averaged overall velocity distribution from all four runners. This shows a non-uniform velocity distribution and an annular area of catalyst that experiences higher mass flow rates. The average flow at the central axis is less than 3.5 m/s whereas the maximum average flow is in excess of 6.5 m/s. Although the diffuser and runners were production components for the 1.4 litre engine under test, it is clear that the velocity distribution achieved in the catalyst is far from ideal. The purpose of this work, however, was not to re-design the system, but to see how well the model could predict observations of velocity in this practical close-coupled system.

4.0 Comparison of measurements with predictions

All tests were performed for approximately 88% of full load at 2000 rpm. The airflow rate to the engine was measured to be 16.34 g/s, and assuming 1.12 g/s of fuel for stoichiometric combustion, the mean exhaust flow velocity at exit from the catalyst should be about 4.0 m/s at 900K.

4.1 Measurements of temporal pulse shapes in runners

The pulse shape was measured in the centre of runner R1 using the LDV system. The measurement is compared with the prediction in Figure 8. On the scale on the abscissa of Figure 8, TDC of cylinder 1 lies at crank angle 360° . It can be seen that the magnitude of the peak velocity is well predicted. Three much smaller peaks are predicted to follow the major peak, but only two are observed. There is agreement, however, in the magnitude of the smaller peaks. The magnitude of the negative flow that follows the major peak is not well predicted. Due to the limitations of the LDV system being used, multiple measurements were made of this negative flow with different filter settings and reversal of the LDV probe. These all confirmed the result presented in Figure 8.

The source of the negative flow that follows the main peak was believed to be caused by reflection from the closed ends of neighbouring runners [9]. The delay between the positive peak and the negative flow, however, is about 40 degrees of crank angle, i.e. 3.3 ms, which corresponds to a pipe length between 1.5 and 2 m, dependent upon temperature. It is likely that reflections are the source of the negative flow but that these are complex and dependent upon the geometry of the system.

The second positive peak is quite broad and probably corresponds to the piston displacement peak that occurs at about 630° crank angle. There are higher frequency pulsations due to pressure harmonics in the system superimposed upon the broad peak.

The discrepancy between the 1D engine simulation and the measured inlet velocity will influence the agreement between the downstream CFD velocity prediction and measured values. This is referred to again in section 4.3 below.

4.2 Cycle-average measurements along axis 3 (60° to normal to engine)

Figure 9 shows the predicted mean (cycle-averaged) velocity profile at the rear of the catalyst along measurement axis 3 compared with measured data. Agreement can be seen to be good near the catalyst centre (diametral location 60 mm). The large velocity peak predicted at about 18 mm from the catalyst wall was not seen in the experiments, where a smaller peak was observed at about 30 mm from the wall. The comparison in Figure 9 is slightly improved on that observed in motored engine experiments [9], where peak displacement was also observed. There is known to be some difficulty in predicting the exact position of the maximum flow, see [15], where a similar problem was encountered in cold flow test rig experiments. Significant swirl from runner R4, mentioned earlier in connection with Figures 6A and 6B, could have a marked effect on the location of the peak in Figure 9. If the swirl in practice is different from that predicted then this would explain the discrepancy in Figure 9 between measurements and predictions.

Another implication of the measurements in Figure 9 is that the mean velocity was higher in the real system in the parts of the flow field that were beyond the reach of the laser probe, i.e. at diametral locations greater than 93 mm, or along other diametral axes. This was thought probable because when the rig was stripped down at the end of the experiments, the staining of the catalyst inlet face was more noticeable on the side nearest the engine, which is consistent with a generally higher flow rate in that region.

4.3 Pulse profiles at catalyst exit along axis 3

Figure 10 compares predicted and measured pulse shapes at the catalyst exit in the region up to 33 mm from the wall. The crank angle scale used in Figures 10 to 12 has 360 ° as TDC of cylinder 1. Both measured and predicted traces consist of a series of four large peaks, due to the blow down, with intervening smaller peaks. The smaller magnitude but temporally broader intervening peak following each blow down peak is the displacement peak, as apparent in the inlet pulse (Figure 8). The large magnitude peak predicted at about 180° crank angle in Figure 10 at locations close to the wall, 8 to 18 mm, is not seen in the measurements. This suggests that the peak area seen in Figure 6A is not located as close to the outer wall in practice as predicted. There is some evidence of temporal broadening of the

peak in the measured trace at 180° at 33 mm from the wall, which is consistent with increased net flow rates occurring farther away from the wall. Measurements were more difficult to obtain at the locations 28 mm and 33 mm, which was attributed to the flow field and the seeding available in this region, and may have indicated high spatial or temporal velocity gradients. In Figure 10, the temporally broadened peak at 540° could suggest that the swirl seen in Figure 6J from runner R1 has reached the point 28 mm from the wall on axis 3 by 570° crank angle. Also, from Figure 10 there appears to be over-prediction of flow velocity from runner 3 near the wall, i.e. at 8, 13 and 18 mm, for 0° crank angle. It appears that the model may not be correctly predicting swirl and its effects in locations close to the outer wall.

Figure 11 compares predicted and measured pulse shapes along axis 3 from 38 mm to 68 mm from the outer wall. Prediction of the peak velocities can be seen to be quite good but the magnitude of the velocity minima is consistently over predicted. This is consistent with over prediction of the magnitude of the minimum in the runner inlet, Figure 8. Near the centre of the catalyst (location 60 mm) there is less fluctuation from location to location in both measurements and predictions, Figure 11, with both exhibiting similar magnitude for the pulses from all four runners.

Figure 12 compares predicted and measured pulse shapes along axis 3 from 73 mm to 88 mm. The discrepancy between measurements and predictions increases again as the measurement point moves further towards the opposite wall of the catalyst. The measured traces show no significant changes in pattern. Some temporal peak broadening at 88 mm might have been expected at 540° from inspection of Figure 6I, which shows significant swirl from runner R1, but Figure 12 shows only that a significant negative velocity is predicted after the peak at 540° at location 88 mm. Again, the magnitude of the negative flow predicted is directly attributable to the large negative flow predicted in the runner, but not seen in the measurements.

Inaccurate prediction of spatial peak location (Figure 9) and temporal peak duration (Figures 10, 11 and 12) is attributable to poor prediction of the swirl from the runners, which in close-coupled catalyst systems have compound bends. The effect is that the area that experiences peak flow is slightly displaced spatially from the predicted location, and in some instances the swirl also affects the length of time over which the flow rate is raised locally.

5.0 Conclusions

A coupled model was used to make predictions for a firing engine. A Star-CD 3D CFD catalyst model and 1D Ricardo WAVE engine cycle simulation model were coupled and predictions were made for a 1.4 litre firing engine at 2000 rpm and 88 % load. Velocities in the range –65 to 240 m/s were predicted in the inlet runners and in range –5 to 22 m/s were predicted downstream of catalyst. Velocities in the range –20 to 240 m/s were observed in the runners using an LDV system. Velocities in the range –2 to 12 m/s were observed downstream of catalyst. There was generally good qualitative agreement between measurements and predictions. The over prediction of the magnitude of the reverse flow in the inlet runner had a direct effect on the predictions of the flow pulses downstream of the catalyst. The measured pulses at the catalyst exit had lower magnitudes of flow reversal than predicted. The flow profile across the exit of the catalyst was well predicted near to the centre of the catalyst but the predicted high mean velocity near the periphery of the catalyst was not observed in the experiments.

The coupled simulation has produced interesting results for a firing engine and work should continue to improve the prediction of the flow in the inlet runner and the flow distribution at the exit from the catalyst. Improve modelling of swirl of flow from runners with compound bends will be required if predictions are to model measurements more closely.

Acknowledgements

We are grateful to ArvinMeritor, who supported the experimental programme with the provision of hardware for the catalyst exhaust system. We also acknowledge assistance with experimental work from Ahmad J. Alimin, and technical support from Martin Hyde of TSI.

References

- [1] Bressler, H., Rammoser, D., Neumaier, H., and Terres, F. Experimental and predictive investigation of a close-coupled catalytic converter with pulsating flow. SAE Paper No. 960564
- [2] Cho, Y-S., Kim, D-S., Han, M., Joo, Y., Lee, J-H., and Min, K-D. Flow distribution in a close-coupled catalytic converter. SAE Paper No. 982552

- [3] **Arias-Garcia A., Benjamin, S. F., Zhao, H., and Farr, S.** A comparison of steady, pulsating flow measurements and CFD simulations in close-coupled catalysts. SAE Paper No. 2001-01-3662. Published in General Emissions in Gasoline Emission Control Systems, SAE SP-1644
- [4] **Arias-Garcia, A.** Investigation of the flow performance of automotive close-coupled catalyst on flow rigs and engines. Coventry University PhD thesis, 2002
- [5] **Zhao, F., Bai, L., Liu, Y., Chue, T., and Lai, M.** Transient flow characteristics inside the catalytic converter of a firing engine. SAE Paper No. 971014. Published in Issues in Emissions Control Technology, SAE SP-1248
- [6] **Benjamin, S. F., Roberts, C. A., and Wollin, J.** A study of pulsating flow in automotive catalyst systems. *Experiments in Fluids*, 2002, **33**, 629 – 639
- [7] **Bai, L., Zhao, F., Liu, Y., Lai, M., and Lee, K.** Transient flow and pressure characteristics inside a close-coupled catalytic converter. SAE Paper No. 982548
- [8] **Park, S-B., Kim, H-S., Cho, K-Y., and Kim, W-T.** An experimental and computational study of flow characteristics in exhaust manifold and CCC (close-coupled catalyst). SAE Paper No. 980128
- [9] **Liu, Z., Benjamin, S. F., Roberts, C. A., Zhao, H., and Arias-Garcia, A.** A coupled 1D/3D simulation for the flow behaviour inside a close-coupled catalytic converter. JSAE Paper No. 20030045. SAE Paper No. 2003-01-1875
- [10] **Fingerson, L. M., and Menon, R. K.** Laser Doppler Velocimetry. Chapter 35, *The Handbook of Fluid Dynamics*, edited by R. W. Johnson, published by CRC press, 1998
- [11] **Haimad, N.** A theoretical and experimental investigation of the flow performance of automotive catalytic converters. Coventry University PhD thesis, 1997

[12] **Zhao, F., Li, L., Xie, X., and Lai, M.** An experimental study of the flow structure inside the catalytic converter of a gasoline engine. SAE Paper No. 950784

[13] **Issa, R. I.** Solution of the implicitly discretised fluid flow equations by operator splitting. *J. Comput. Physics*, 1986, **62**, 40 -65

[14] *Star-CD Users Guide and Methodology*, 2001 (Computational Dynamics Limited)

[15] **Benjamin, S. F., Zhao, H., and Arias-Garcia, A.** Predicting the flow field inside a close-coupled catalyst – the effect of entrance losses. *Proc. Instn. Mech. Engrs. Part C (J Mech Eng Science)*, 2003, **217**, 283 - 288

TABLES (Captions listed overleaf)

Table 1

| Signal frequency (MHz) | Velocity (m/s) |
|------------------------|----------------|
| 5 | -19.35 |
| 10 | 0 |
| 20 | 38.7 |
| 30 | 77.4 |
| 90 | 309.6 |

Table 2

| Runner | Exhaust | EVC | BDC | IVC | Compress. | EVO | BDC | IVO | Exhaust |
|--------|---------|-----|-----|-----|-----------|-----|-----|-----|---------|
| No. | TDC | | | | TDC | | | | TDC |
| 1 | 0 | 23 | 180 | 242 | 360 | 501 | 540 | 698 | 720 |
| 3 | 180 | 203 | 360 | 422 | 540 | 681 | 720 | 158 | 180 |
| 4 | 360 | 383 | 540 | 602 | 720 | 141 | 180 | 338 | 360 |
| 2 | 540 | 563 | 720 | 62 | 180 | 321 | 360 | 518 | 540 |

CAPTIONS FOR TABLES

Table 1 Velocity and signal frequency for LDV system

Table 2 Valve timing for 1.4 litre engine

List of Figure Captions

Figure 1

Schematic diagram, showing plan of catalyst monolith as viewed from the exit, with axes of measurement and relative locations of runner entries (R1 to R4).

Figure 2

Photograph of the test rig.

Figure 3

Schematic of the 1D WAVE model for the coupled 1D/3D simulation, reproduced from [9].

Figure 4

CFD mesh of the close-coupled catalyst system, showing the four inlet runners (1 to 4) and the outlet boundary (5); reproduced from [9].

Figure 5

Predicted mean velocity profiles at catalyst exit. Location is measured from catalyst wall so 60 mm approx. is centre and 120 mm is far wall.

Figure 6 [A] to [D]

Contour plots of instantaneous velocity predicted for exit of catalyst (direction of view indicated).

Blow down pulse seen above originates from R4 and peaks just after 180 deg.

Figure 6 [E] to [H]

Contour plots of instantaneous velocity predicted for exit of catalyst (direction of view indicated).

Blow down pulse seen above originates from R2 and peaks just after 360 deg.

Figure 6 [I] to [L]

Contour plots of instantaneous velocity predicted for exit of catalyst (direction of view indicated).

Blow down pulse seen above originates from R1 and peaks just after 540 deg.

Figure 6 [M] to [P]

Contour plots of instantaneous velocity predicted for exit of catalyst (direction of view indicated).

Blow down pulse seen above originates from R3 and peaks just after 720 deg (0 deg).

Figure 7

Simulated cycle-averaged velocity distribution at exit from catalyst. Scale range is 0 to 7 m/s with a local maximum of 6.9 m/s. Engine operating condition, 2000 rpm and 88% full load. Angle of view indicated.

Figure 8

Predicted velocity in inlet runner R1 compared with data; compression TDC in the associated cylinder is at 540 degrees.

Figure 9

Comparison of mean velocity profile predicted for Axis 3 at rear of catalyst compared with measured data.

Figure 10

Predicted and measured pulses at catalyst exit at diametral locations 8, 13, 18, 28 and 33 mm from outer wall.

Figure 11

Predicted and measured pulses at catalyst exit at diametral locations 38, 48, 58, 63 and 68 mm from outer wall.

Figure 12

Predicted and measured pulses at catalyst exit at diametral locations 73, 78, 83 and 88 mm from outer wall.

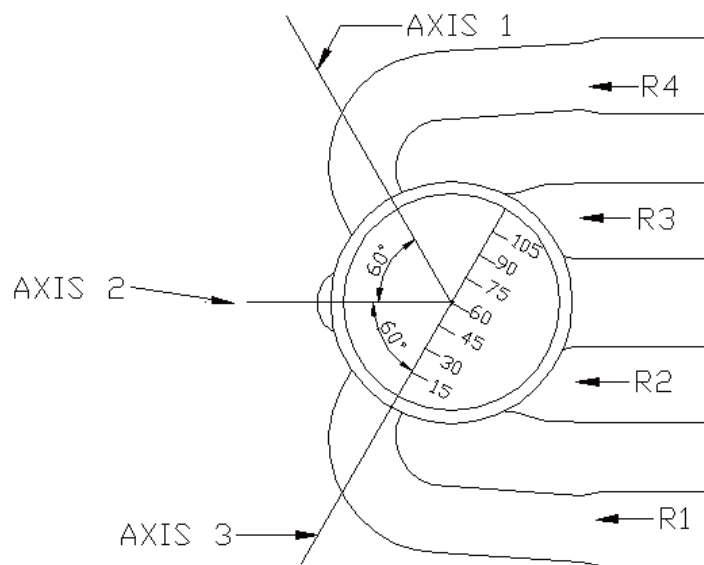


Figure 1



Figure 2

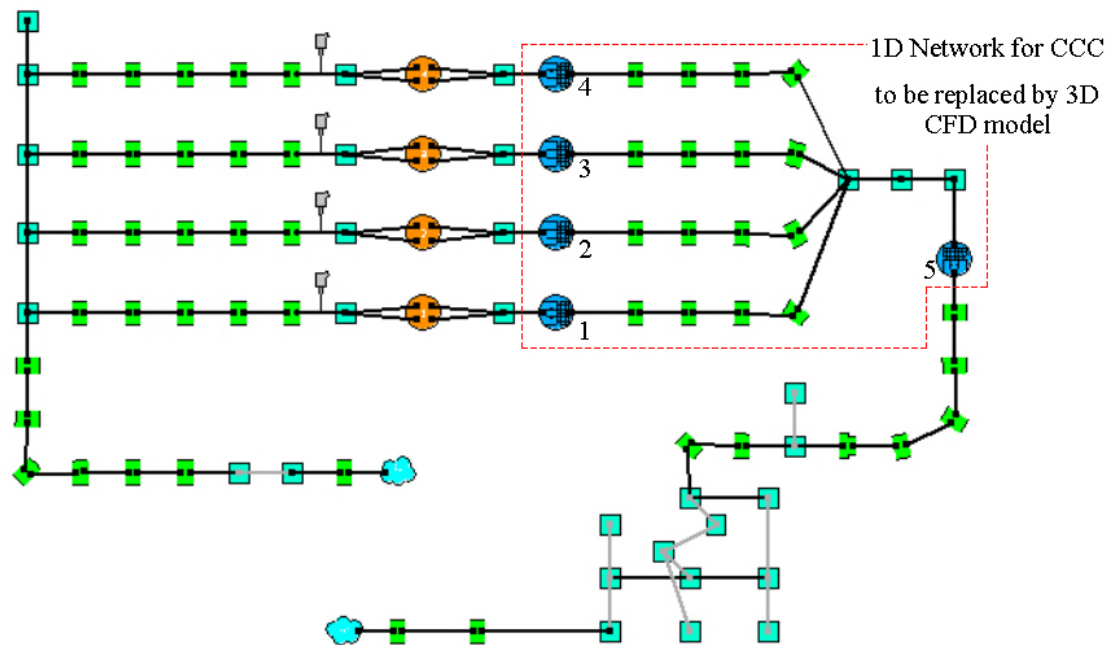


Figure 3

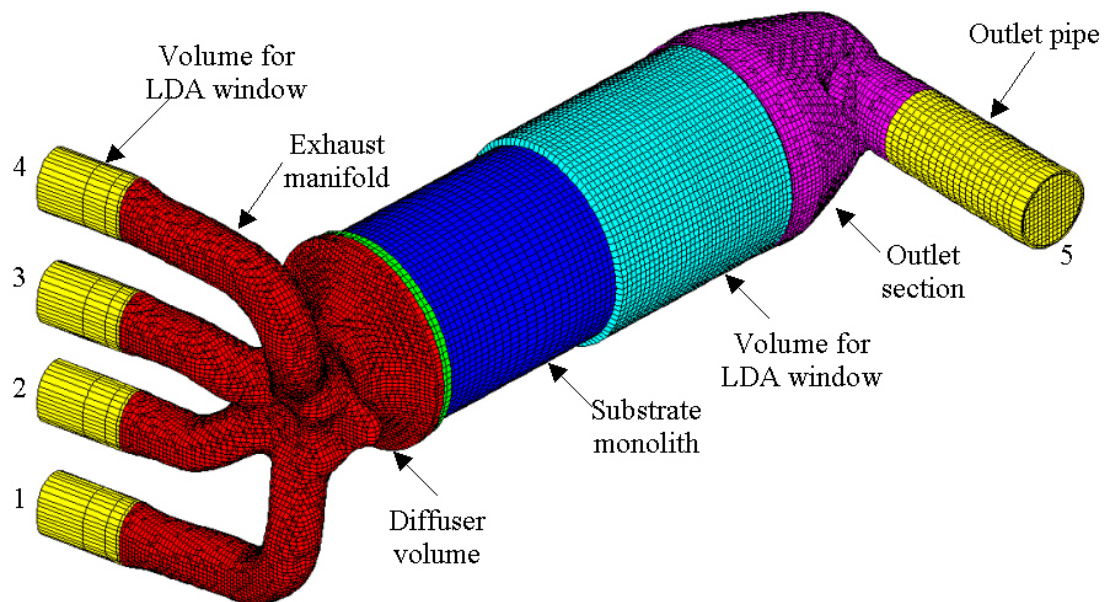


Figure 4

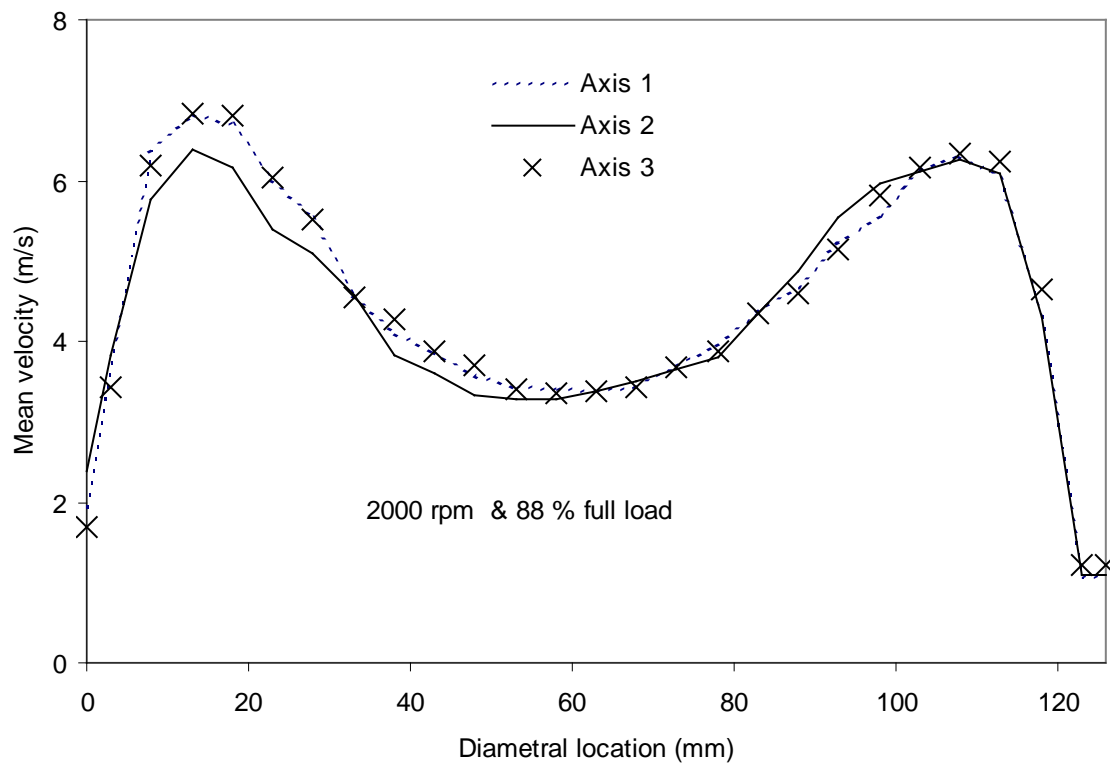
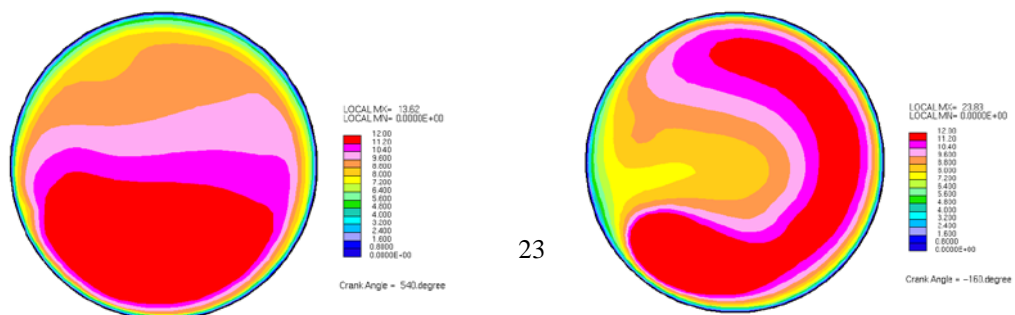
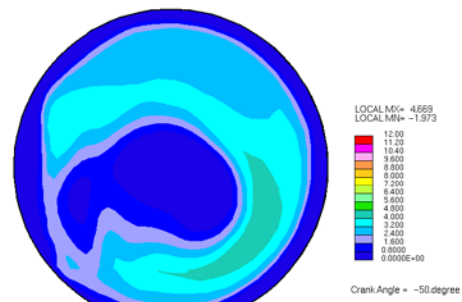
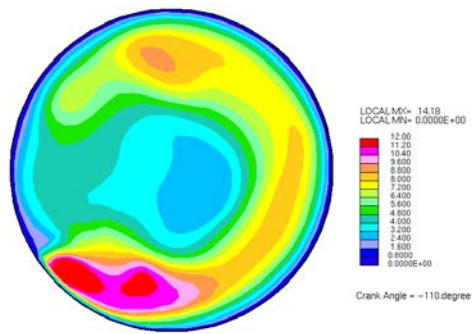


Figure 5



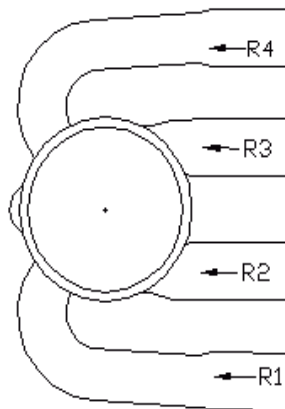
[A] 180 deg (Comp TDC of Cylinder 2)

[B] 200 deg

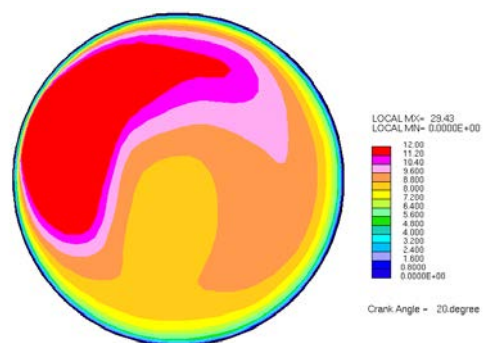
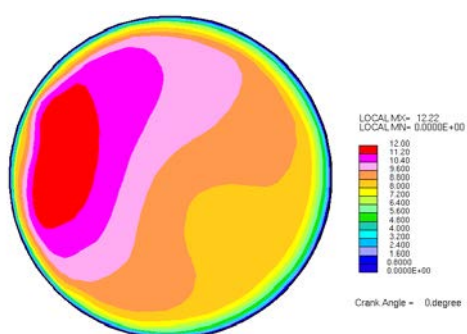


[C] 250 deg

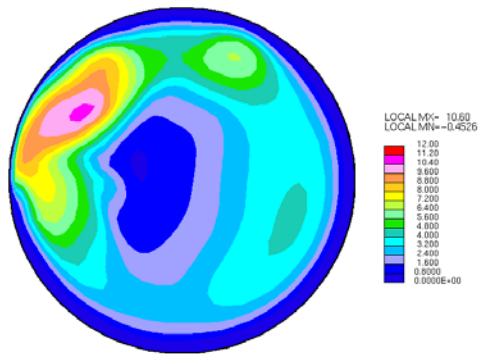
[D] 310 deg



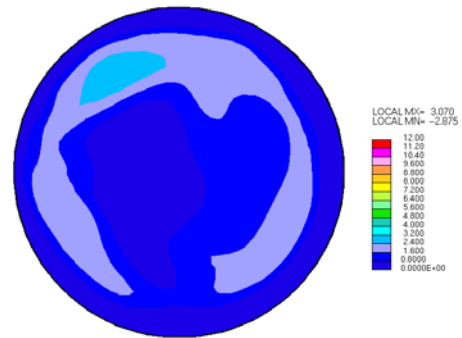
Figures 6A – 6D



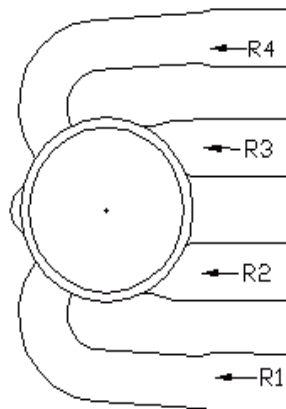
[E] 360 deg (Comp TDC of cylinder 1)



[F] 380 deg

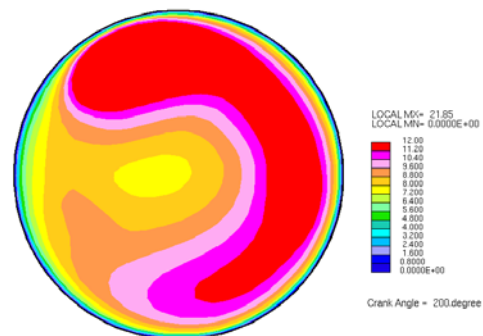
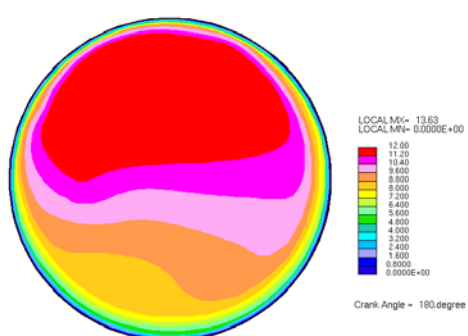


[G] 430 deg

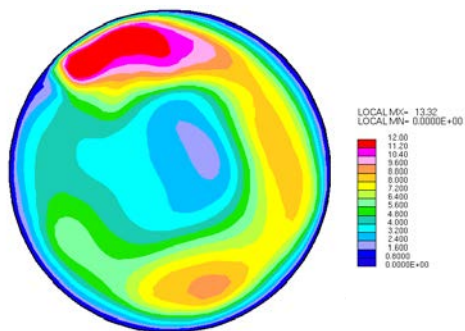


[H] 480 deg

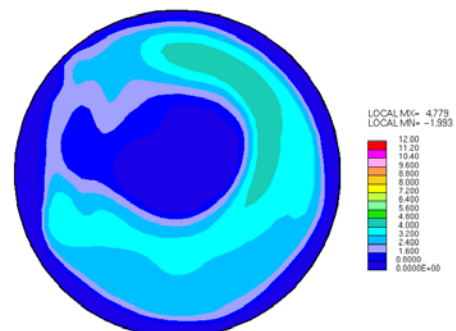
Figures 6E – 6H



[I] 540 deg (Comp TDC of Cylinder 3)

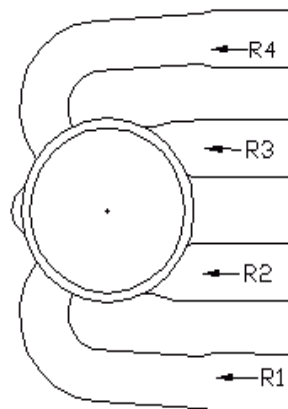


[J] 560 deg

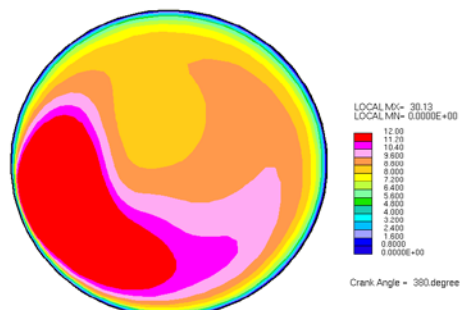
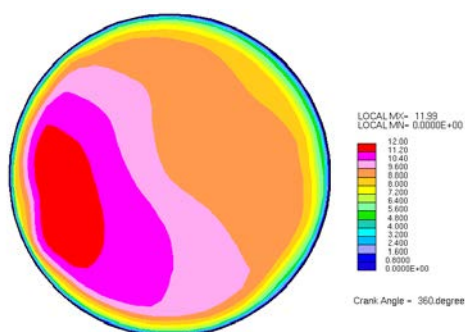


[K] 610 deg

[L] 670 deg

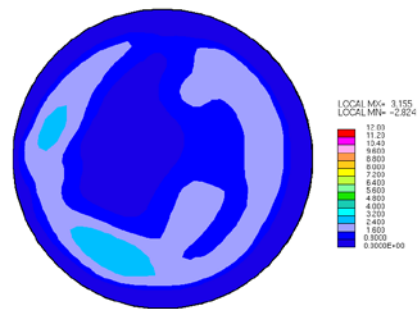
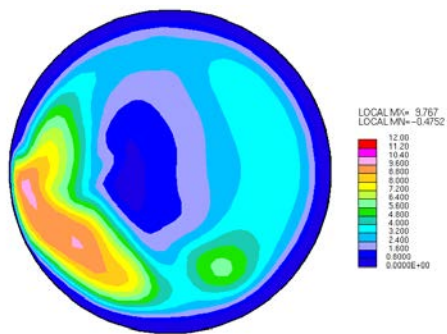


Figures 6I – 6L



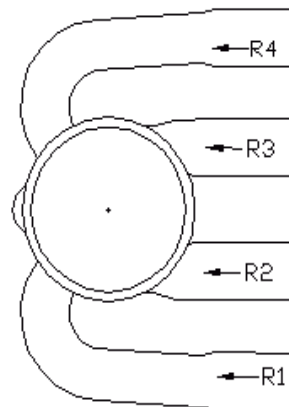
[M] 720 deg & 0 deg (TDC comp of cylinder 4)

[N] 20 deg



[O] 70 deg

[P] 120 deg



Figures 6M – 6P

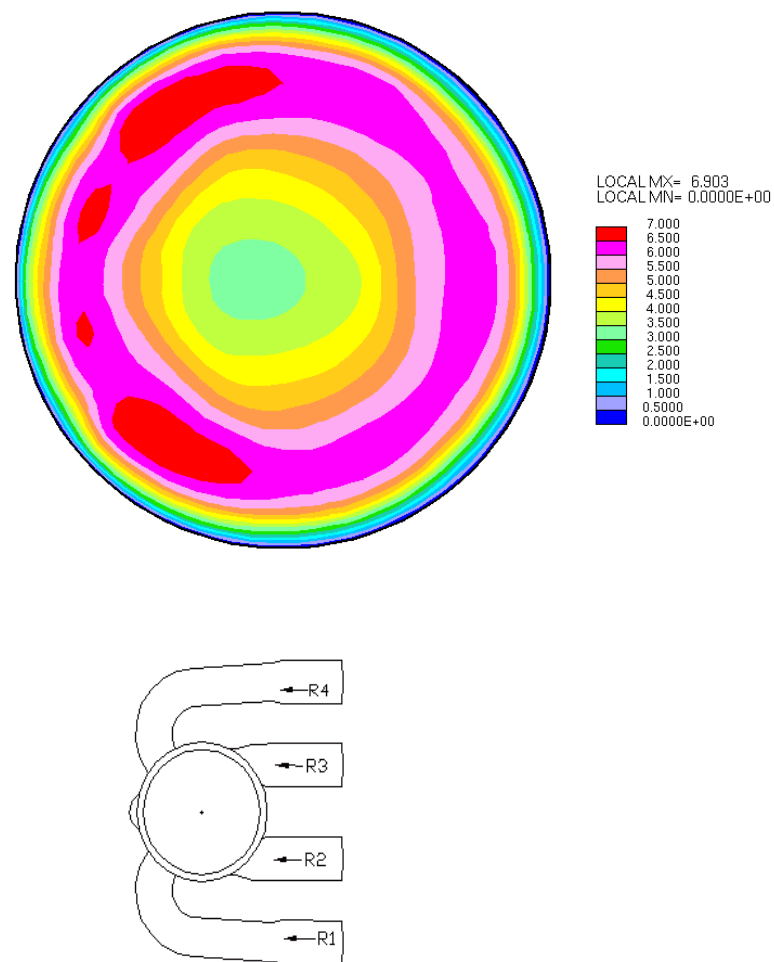


Figure 7

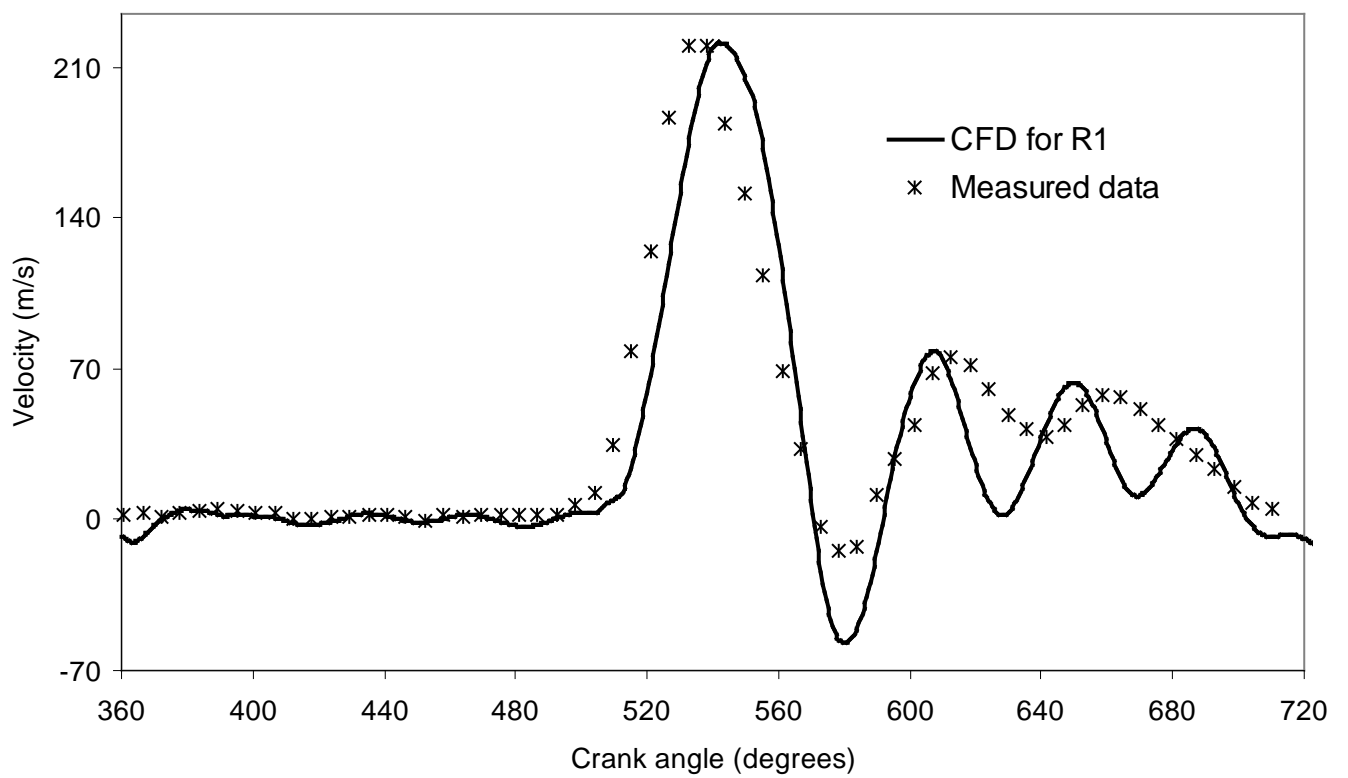


Figure 8

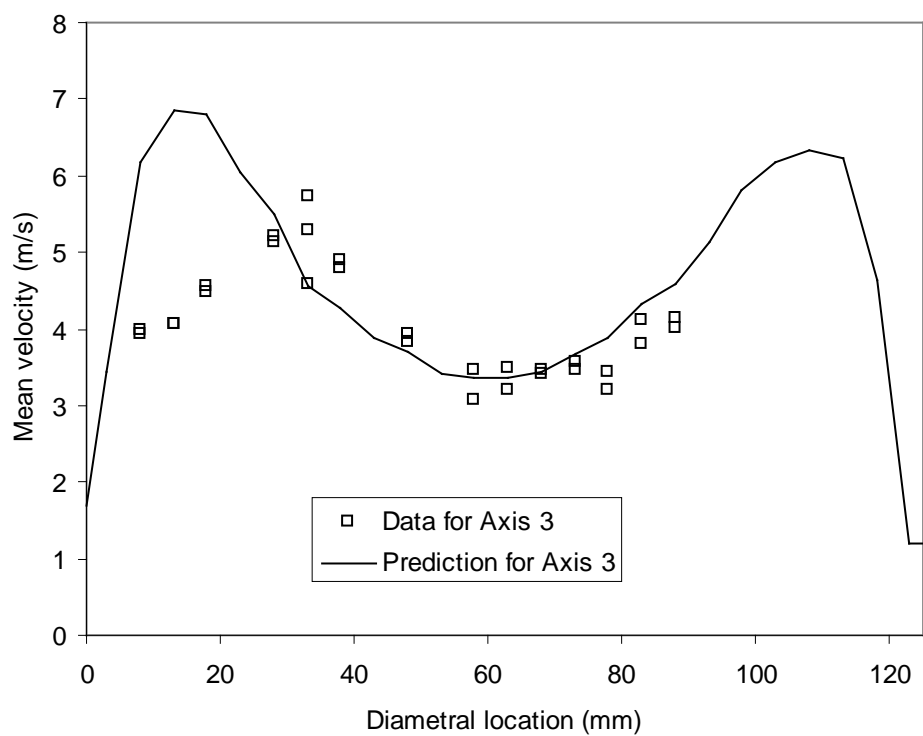


Figure 9

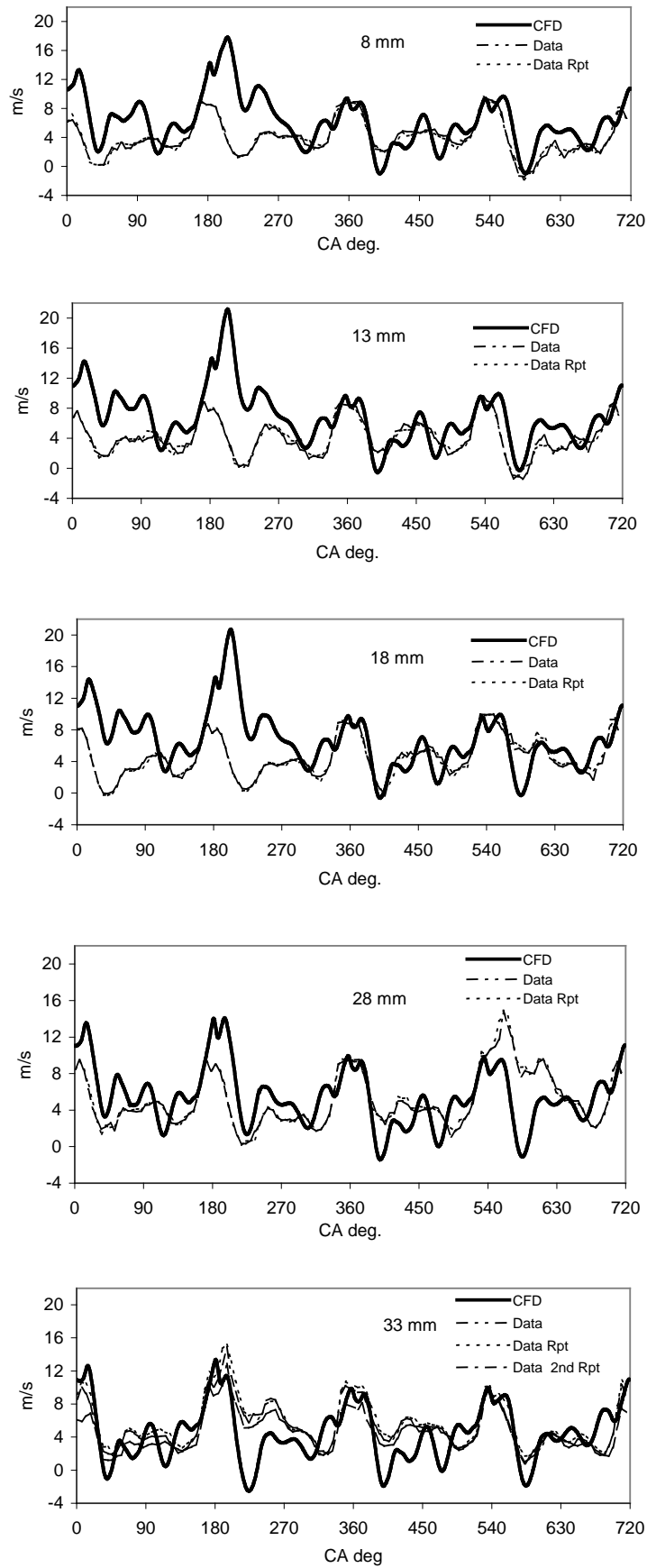


Figure 10

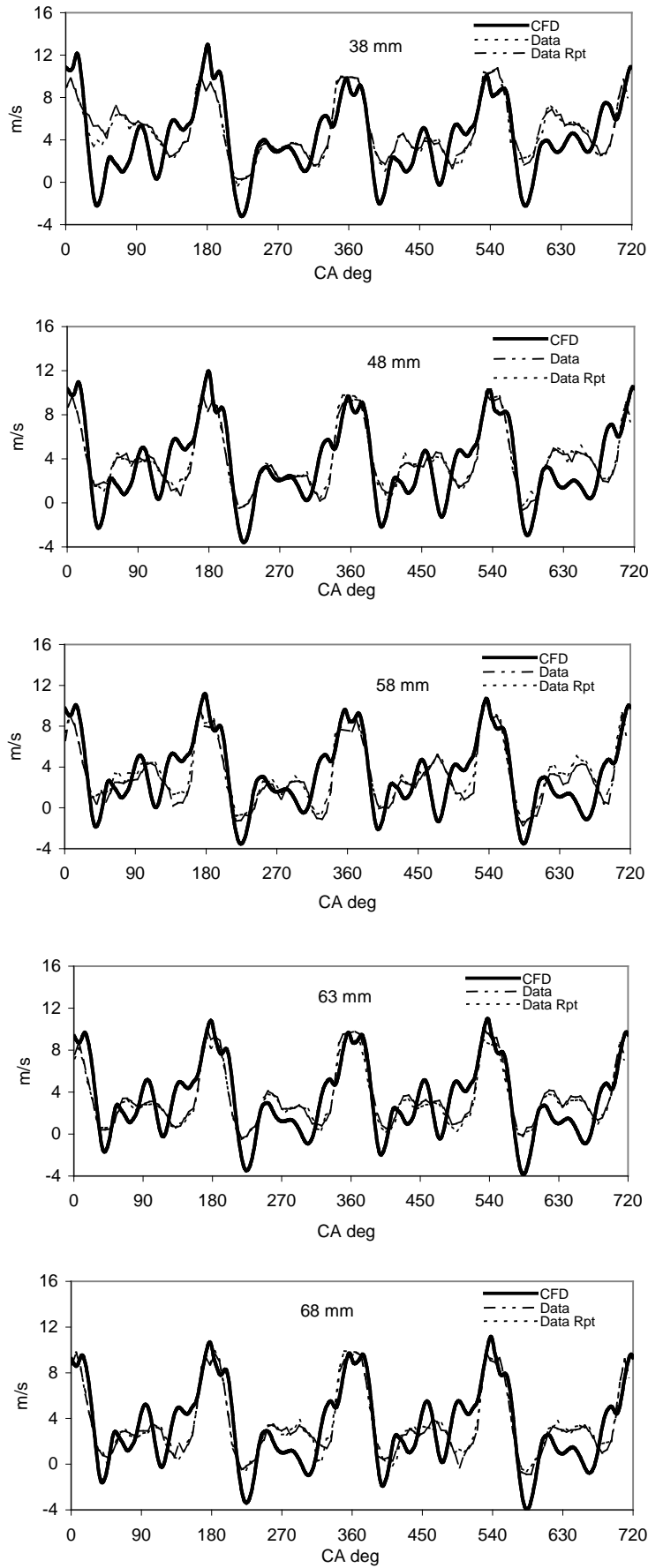


Figure 11

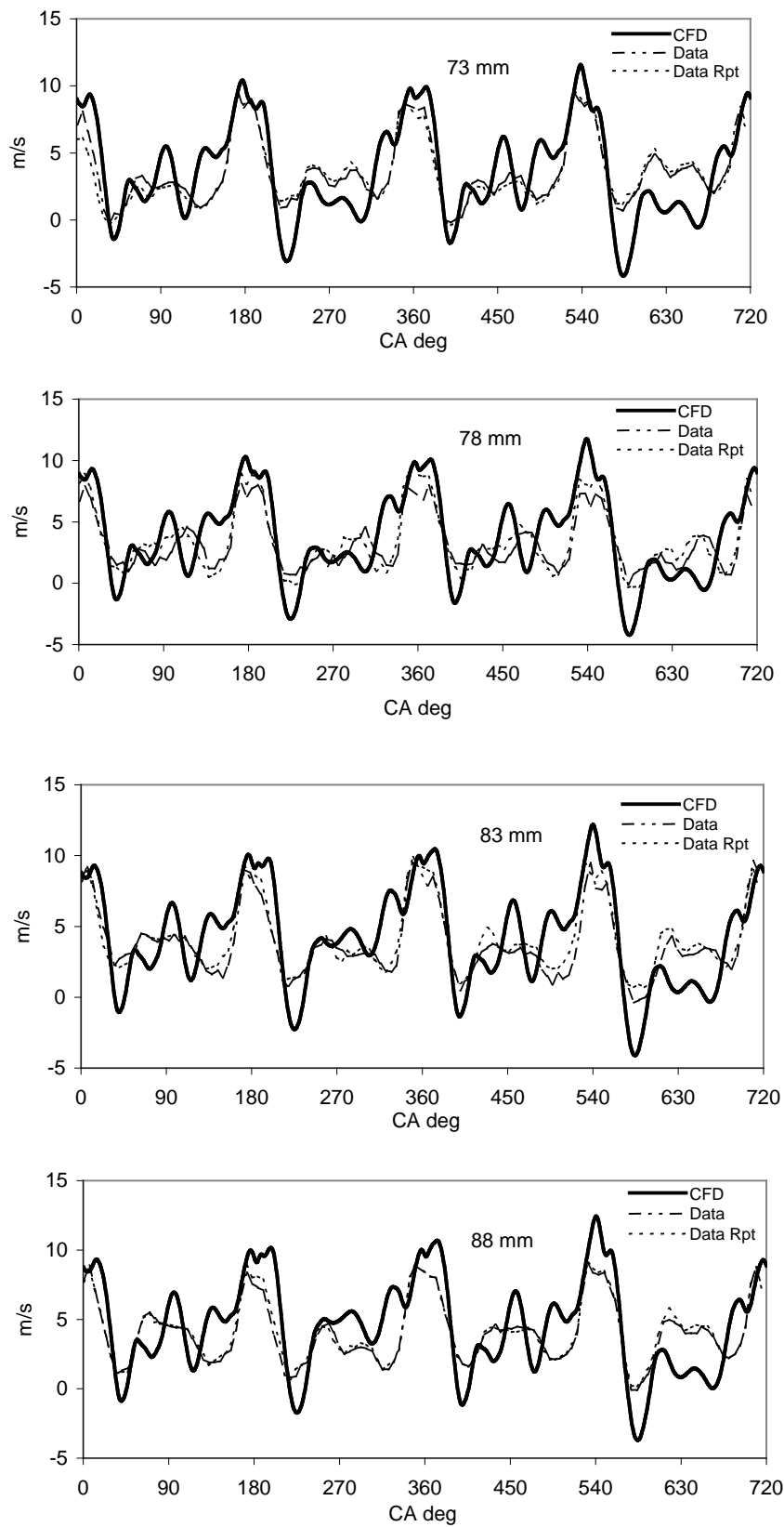


Figure 12

